ADVANCED FUNCTIONAL MATERIALS
www.afm-journal.de

Improved Thermal Stability of Polymer Solar Cells by Incorporating Porphyrins

Sisi Wang, Yunpeng Qu, Sijun Li, Feng Ye, Zhaobin Chen, and Xiaoniu Yang**

Thermal stability has been the important issue in organic solar cell, especially for the large scale fabrication and application in the future. In this work, a new strategy involving the introduction of porphyrin compound (BL) is proposed to prevent the [6,6]-phenyl C61 butyric acid methyl ester ($PC_{61}BM$) aggregation. The supramolecular interactions between $PC_{61}BM$ and BL are first demonstrated in $PC_{61}BM$:BL binary blend, and then the effect of BL on P3HT:$PC_{61}BM$ blend is qualitatively and quantitatively studied by differential scanning calorimetry, UV–vis absorption spectroscopy, atomic force microscopy, optical microscopy, and fluorescence techniques. It is found that the BL addition not only stabilizes the morphology of P3HT:$PC_{61}BM$ blend films, but also shows a good ability to maintain the electron mobility by depressing the $PC_{61}BM$ crystallization. And the thermal stability of the devices based on P3HT:$PC_{61}BM$:BL ternary blend films is therefore greatly improved. For example, 8 wt% BL doping drops the power conversion efficiency by 10.5% relative to its peak value after 48 h of annealing at 130 °C, while 71.5% of decrease is obtained for the device without BL after only 3 h of annealing. This strategy is preliminarily proved to be universal and will show great potentials in future commercialization of polymer solar cells.

1. Introduction

Polymer solar cells (PSCs) based on solution-processed bulk-heterojunctions (BHJs) have been a world-wide field of interest as a source of renewable energy with outstanding advantages, such as low cost, light weight, and flexibility, as well as large-area feasibility.[1] Single BHJ structure has demonstrated the efficiency of up to ≈9%,[2] whereas for tandem BHJ structure this value exceeds the 10% watershed.[3] Although a variety of low-band gap polymers has been the hot topic in the past two decades, the traditional BHJ structure composed of poly(3-hexylthiophene):phenyl-C61-butyric acid methyl ester (P3HT:$PC_{61}BM$) is still the typical system used as the research model for organic photovoltaics due to its stability and reliable material source.[4] In addition, P3HT:$PC_{61}BM$ is also one of the most promising candidates until now for large-scale production because of the commercial availability and easy processing in air. For example, Krebs presented the fully printed polymer solar cell modules based on P3HT:$PC_{61}BM$.[5]

Although the power conversion efficiency (PCE) is the parameter that the researchers are most interested in, the stability of the device must be taken into consideration because it is directly related to the life time of PSC. It is now recognized that PSC stability depends on interface material issues, photodegradation of organic materials and morphological stability of the blends.[6] The first two issues could be solved by optimizing fabrication technologies,[7] while the last one is induced by internal driving force (phase segregation), extrinsic technological optimization is hardly helpful. An appropriate phase segregation is necessary for exciton dissociation,[8] while excessive phase segregation, which could be accelerated by the accumulated heat from the long-term sunlight irradiation in real application,[9] will dramatically decrease the interface area, increase the exciton recombination,[10] and thus bring negative effect on the device efficiency. Even in stable P3HT:$PC_{61}BM$ blends, the issue of morphological instability induced by thermal stress should not be underestimated, because semicrystalline P3HT tends to expel $PC_{61}BM$ during its crystallization, and $PC_{61}BM$ molecules aggregate due to the strong driving force for crystallization.

Currently, much effort has been made by a number of research groups to stabilize the active layer morphology and some methods, for example, decreasing the crystallinity of polythiophenes,[11] constructing densely distributed P3HT nanofibers,[12] adopting amorphous fullerene electron acceptor,[13] introducing compatibilizer,[14] cross-linking,[15] and other techniques restricting the movement of acceptor molecules,[16] have been developed and substantially improved the morphological stability of the BHJ-based solar cells.

Porphyrin is an attracting family of compounds that could interact with other compounds, like fullerenes, to form complexes due to π–π interactions or Van der Waals forces.[17] This supramolecular interaction could be established universally and easily between porphyrins and fullerenes with no need of special conditions. In organic photovoltaics, it was reported that porphyrins and their derivatives could also be introduced into devices as photosensitizing agents due to their easy syntheses, high extinction coefficients, and broad absorption spectra.[18] Based on these pioneering studies, the authors associate that

S. Wang, Dr. Y. Qu, Dr. S. Li, F. Ye,
Prof. Z. Chen, Prof. X. Yang
State Key Laboratory of Polymer Physics and Chemistry
Changchun Institute of Applied Chemistry
Chinese Academy of Sciences
5625 Renmin Street, Changchun, Jilin 130022, P.R. China
E-mail: zhaobinchen@ciac.ac.cn; xnyang@ciac.ac.cn

DOI: 10.1002/adfm.201403018

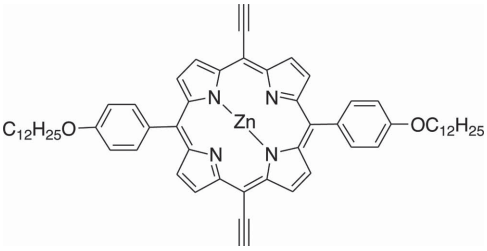

Scheme 1. Chemical structure of BL.

the fullerene derivatives, such as $PC_{61}BM$, which is widely used as the acceptor in polymer solar cells, could interact with porphyrins and thus the thermal stability of the devices should be improved due to the inhibition of $PC_{61}BM$ aggregation. To the best of our knowledge, this has never been reported before.

In this paper, the (zinc-5, 15-diethynyl-10, 20-di(4-dodecyloxyphenyl) porphyrin, named as BL (**Scheme 1**), was selected to demonstrate this novel strategy. Here, it should be noted that the porphyrin solution we used in this work must be prepared freshly due to the photochemical instability relative to the BL in solid state or blend film (Figures S1–S3, Supporting Information). First of all, the BL-$PC_{61}BM$ interaction was verified in BL:$PC_{61}BM$ binary system in terms of spectroscopy and morphology. Then, the supramolecular interactions of BL with $PC_{61}BM$ were investigated in P3HT:$PC_{61}BM$:BL ternary system, and the relationship between porphyrin content and ability to inhibit $PC_{61}BM$ aggregation was studied in detail. Finally, the effect of BL on the performance and electron mobility of photovoltaic devices based on P3HT:$PC_{61}BM$ blend film was provided and the mechanisms were elucidated.

2. Results and Discussion

2.1. Supramolecular Interaction between $PC_{61}BM$ and BL

According to previous reports, the presence of the supramolecular interactions (electronic interactions in nature) between porphyrin and fullerene could be detected by UV–vis spectroscopy.[19] As an illustration, the spectrum of BL:$PC_{61}BM$ blend solution is depicted in **Figure 1**a together with the spectra of BL and $PC_{61}BM$ for comparison. It can be seen that the absorption spectrum of BL in *o*-dichlorobenzene (ODCB) changes upon the addition of $PC_{61}BM$ (about 2 equivalent of BL), and the absorption of the Soret band is red shifted ($\Delta\lambda$ = 8 nm) and broadened. This similar bathochromic-shift of absorption has been demonstrated to relate to the face-to-face porphyrin-fullerene complexes.[20]

In conformationally flexible porphyrin/fullerene dyads, π-stacking interactions facilitate the throughspace attraction between the flat tetrapyrrole ring and the curved surface of the fullerene, which is accompanied by the formation of fullerene-excited states (by energy transfer) or generation of porphyrin$^+$/fullerene$^-$ ion-pair states (by electron transfer) and could be demonstrated by fluorescence quenching technique.[21] Figure 1b shows the curves of quenched BL solutions upon addition of $PC_{61}BM$, showing the dramatically decreased band intensities at 640 and 684 nm with the $PC_{61}BM$ introduction, which indicates the presence of the photo-induced energy transfer or electron transfer from BL to $PC_{61}BM$ due to the formation of BL/$PC_{61}BM$ complexes, although we could not figure out which one of them dominates at this stage. The red-shift in UV–vis spectra and the decreased intensity of BL peaks in fluorescence spectra reveal that the BL could interact with $PC_{61}BM$ to form complex due to the supramolecular interactions and the electronic structure of BL is perturbed to some extent upon blending with $PC_{61}BM$.

The presence of the supramolecular interaction between BL and $PC_{61}BM$ will bring effect on the crystallization of $PC_{61}BM$, and thus change the crystallization behavior of $PC_{61}BM$, as shown in **Figure 2**, which gives the optical images of neat $PC_{61}BM$, neat BL, and $PC_{61}BM$:BL blend films with different blending ratios before and after annealing. In order to better resolve the small crystallites and assign the crystals, the blend films are also investigated by atomic force microscopy (AFM) and X-ray diffraction (XRD), shown in Figures S4 and S5, Supporting Information, separately. Figure 2a shows that the homogeneous $PC_{61}BM$ film is formed during the spin-coating process, while after annealing at 150 °C for 1 h, numerous needle-shaped micro-scale $PC_{61}BM$ crystals are formed, and the surface roughness of height image increases sharply to 211 nm from initial 0.4 nm (Figure S4a, Supporting Information). Once BL introduced ($PC_{61}BM$:BL = 1:0.2, by weight), as expected, it could interact with $PC_{61}BM$ and depress the $PC_{61}BM$ crystallization. Although the pristine $PC_{61}BM$:BL blend film does not show differences in morphology in comparison with the neat

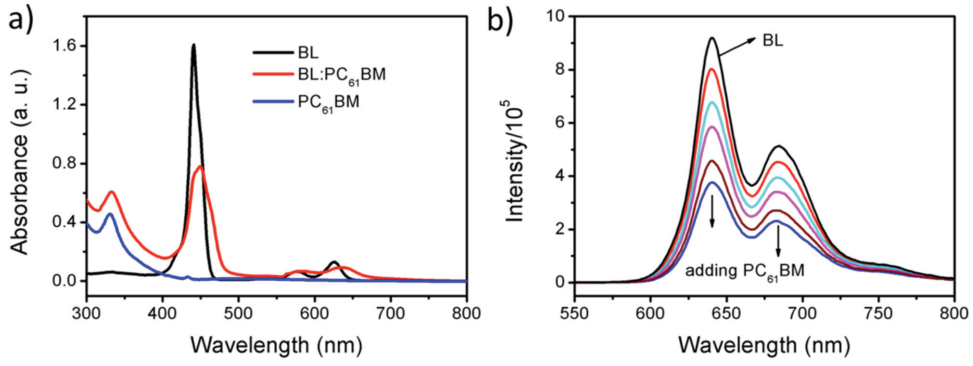

Figure 1. a) UV–vis absorption spectra of BL, $PC_{61}BM$ and BL:$PC_{61}BM$(1:2, w/w) blend in ODCB. b) Curves of quenched BL solutions (2.6×10^{-5} M) in ODCB upon addition of $PC_{61}BM$ with different concentrations (0–2.61×10^{-5} M) (excited at 426 nm).

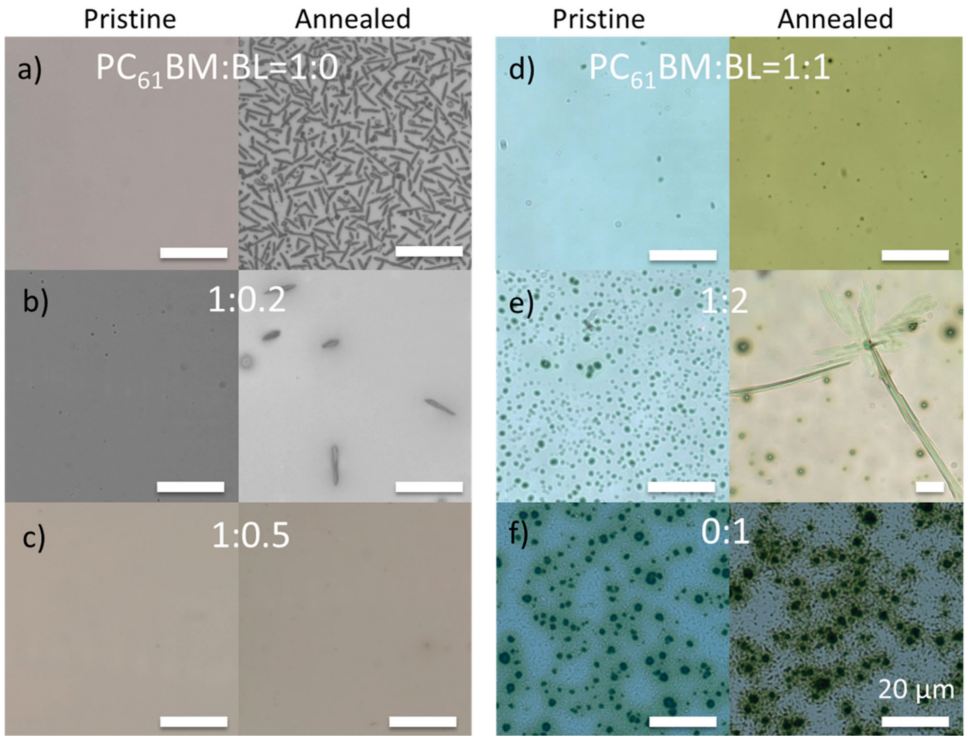

Figure 2. OM images before and after isothermal heating at 150 °C for a) $PC_{61}BM$ (1 h), b) $PC_{61}BM$:BL = 1:0.2 (36 h), c) $PC_{61}BM$:BL = 1:0.5 (36 h), d) $PC_{61}BM$:BL = 1:1 (36 h), e) $PC_{61}BM$:BL = 1:2 (36 h), and f) BL (1 h). Scale bar is 20 μm.

$PC_{61}BM$, the annealed blend film shows much less $PC_{61}BM$ crystals (Figure 2b). If BL increases to an appropriate amount ($PC_{61}BM$:BL = 1:0.5 in this case), no $PC_{61}BM$ crystals are observed both for pristine and annealed blend films, and the surface of the film keeps smooth (1.27 nm of roughness) even after 36 h of heating (Figure S4c, Supporting Information), which indicates that the BL molecules are fully dispersed in and interacted with $PC_{61}BM$ molecules at this point, and the crystallization of $PC_{61}BM$ is greatly depressed by supramolecular interactions between $PC_{61}BM$ and BL.

However, over-loaded BL would negatively influence the morphology of $PC_{61}BM$:BL blend film. For example, the round shape aggregates are clearly observed both in pristine $PC_{61}BM$:BL(1:1) and $PC_{61}BM$:BL(1:2) blend films (Figure 2d,e), which are mainly BL aggregates deduced from the comparison with the neat BL film (Figure 2f). The size of the BL aggregates grows with increasing BL content: nanometer for the former and micrometer for the latter (Figure S4d,e, Supporting Information). Thermal annealing also promotes the formation of large size BL crystals, especially in the case of $PC_{61}BM$:BL(1:2) blend, the BL crystals as long as hundreds of micrometers can be observed in Figure 2e. From above descriptions, it is found that the appropriate BL content is very important for the formation of homogeneous and thermally stable blend films.

2.2. Supramolecular Interactions in P3HT:$PC_{61}BM$:BL Ternary System

The interactions of BL with $PC_{61}BM$ in BL:$PC_{61}BM$ binary system have been demonstrated above. However, whether the electron donor in a typical active layer of the polymer solar cells affects or interferes the interaction between BL and $PC_{61}BM$ is unclear. In this section, a series of P3HT:$PC_{61}BM$ blend films containing 0%, 4%, 8%, and 16% of BL (relative to $PC_{61}BM$ weight) is prepared and the influence of BL on P3HT:$PC_{61}BM$ blend is investigated.

The morphology evolution of P3HT:$PC_{61}BM$:BL blend films with thermal annealing is first monitored by optical microscopy (OM), as shown in **Figure 3**, from which it can be seen that the morphology of P3HT:$PC_{61}BM$ blend film without BL is most sensitive to thermal annealing: macrographic phase separation appears after 25 min, evolves as time going, and finally fixes after 3 h. During this process, the size and the number of $PC_{61}BM$ crystals gradually increase, and the final $PC_{61}BM$ crystals are round-like in few micrometers. Apparently different, the macrographic alteration of P3HT:$PC_{61}BM$:BL blend films upon thermal annealing is mitigated by incorporating BL. All the BL-loaded blend films maintain uniform micrographic morphology after initial 25 min of thermal annealing, and the morphology alteration correlates to BL content: as the BL content increases, the time for phase separation prolongs, and the separated $PC_{61}BM$ crystals become less and larger. We attribute these changes to the difficulty in nucleation and diffusion of $PC_{61}BM$ molecules due to the physical BL-$PC_{61}BM$ interactions.[22] Considering the facts that the porphyrin with ethyne groups could take the cross-linking reaction[23] and the cross-linking is the reason to improve the morphology in some cases,[24] the studies on the solubility, Fourier transform infrared spectroscopy (FTIR), and thin layer chromatography (TLC) of the thermally stabilized film, were conducted (Figures S6–S8, Supporting

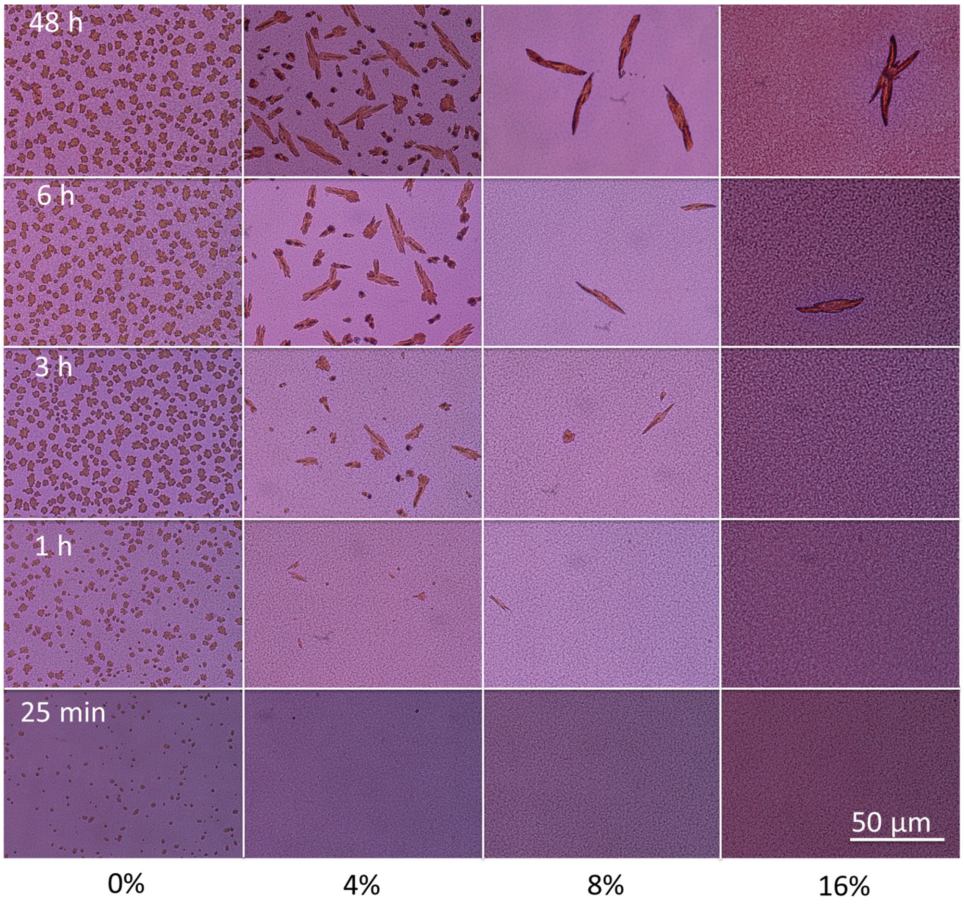

Figure 3. OM images of morphological evolution of P3HT: $PC_{61}BM$ blend films with different BL content and thermal annealing times (thermal annealing temperature is 130 °C, scale bar is 50 μm).

Information). It is found that the cross-linking did not happen during the whole thermal annealing process, further indicating the physical interactions between BL and PCBM.

To gain quantitative analysis about the influence of BL content on the morphological evolution, the absorption of $PC_{61}BM$ in P3HT:$PC_{61}BM$ blend films with or without BL as thermal annealing time is also monitored by UV–vis absorption spectra (**Figure 4**).[25] The UV–vis spectra were recorded at 0 min, 10 min, and then at intervals of 20 min from 20 to 100 min and at intervals of 30 min from 100 to 280 min, and finally at 2440 and 3580 min, respectively. The films were transferred immediately to cool aluminum plate as soon as reaching the time point and allowed to stand for 10 min to freeze the morphology. Moreover, the films were fixed by a predesigned locating equipment to ensure that the incident light penetrates the same position of the film in every measurement. As shown in Figure 4, the value of absorbance of all the blends at 335 nm decreases and background absorbance strengthens as heating time prolongs. Upon thermal annealing, $PC_{61}BM$ molecules are thermally driven to aggregate, which promotes the formation of inhomogeneous morphology composed of P3HT rich domains and $PC_{61}BM$ aggregates. On one hand, the incident light readily penetrates the transparent P3HT rich regions, leading to high transmission at 335 nm. On the other hand, the $PC_{61}BM$ aggregates are fully opaque to the spectrometer and even large enough to scatter the incident light, leading to less transmitting at full range. Therefore, it is believed that it is the aggregation of $PC_{61}BM$ that results in the changes of absorbance, which corroborates the unstable blend morphology. A detailed insight into the UV–vis spectra reveals that the absorbance curves almost unchanged (two curves coincide) when the thermal annealing time is prolonged from 2440 to 3580 min, which indicates that the blend film arrives at a relatively stable state. At this state, the peak at 335 nm in the absorbance curve of P3HT:$PC_{61}BM$ blend film nearly disappears, while the one of the BL-contained film goes sharper as the BL content raises. This distinction illustrates less $PC_{61}BM$ aggregate with higher content of BL.

Figure 4 also states that the varying rate of absorbance at 335 nm decelerates as BL content increases. To compare quantitatively, the decreasing rate of peak intensity at 335 nm is calculated by I_{PCBM}/I_0 (where I_0 and I_{PCBM} are the intensities of the incidence light at λ = 335 nm and $PC_{61}BM$ absorption, respectively. I_{PCBM}/I_0 was calculated according to Equations and illustrated in the Supporting Information), and the values obtained are plotted against time, as shown in **Figure 5**a. Normally, a standard "S" curve composed of gentle nucleation, rapid growth, and gentle equilibrium periods should be present.[22] For P3HT:$PC_{61}BM$:BL system, however, the absorption of $PC_{61}BM$ with annealing time strongly depends on

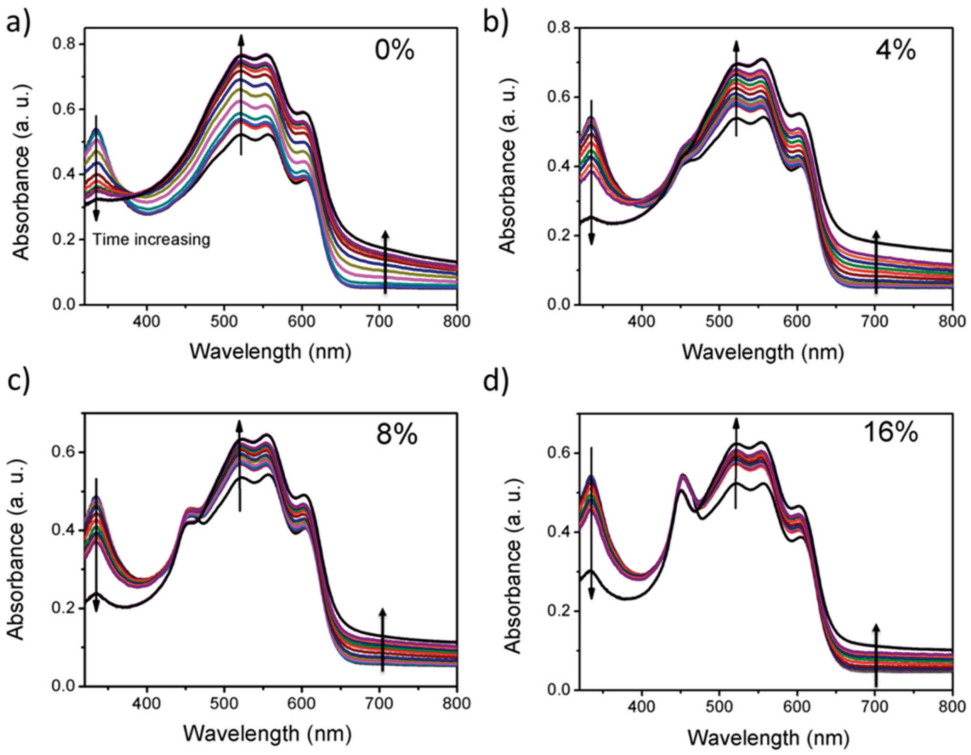

Figure 4. UV–vis absorption spectra of P3HT:$PC_{61}BM$ films with different amounts of BL annealed at 130 °C for different times: a) P3HT:$PC_{61}BM$, b) P3HT:$PC_{61}BM$:BL (4%), c) P3HT:$PC_{61}BM$:BL (8%), and d) P3HT:$PC_{61}BM$:BL (16%). Arrow indicates the time increasing direction.

BL amount. For example, the P3HT: $PC_{61}BM$ blend does not show the gentle nucleation process because this process has been finished in a short time (less than 40 min) due to the quick aggregation of $PC_{61}BM$. The BL addition brings out the nucleation process, which is closely related to the BL amount. For instance, the nucleation period is between 40 and 60 min for P3HT:$PC_{61}BM$:BL (4% and 8%) blend films, while longer than 100 min for the P3HT:$PC_{61}BM$:BL (16%) blend films. In other words, the supramolecular interactions between $PC_{61}BM$ and BL inhibit the $PC_{61}BM$ crystallization and prolong the $PC_{61}BM$ nucleation period. The other effect of the BL addition is to increase the time reaching the equilibrium period: from 200 min for P3HT:$PC_{61}BM$ blend film to longer than 280 min for P3HT:$PC_{61}BM$:BL (16%) blend film.

The rate of the $PC_{61}BM$ crystallization could be reflected from the slope of the growth period (second section) in the "S" curve, which dominates the whole crystallization process. By linear fitting with an $R > 0.99$, the slope of 1.69×10^{-3} is obtained for P3HT:$PC_{61}BM$ blend film, which is higher than that of P3HT:$PC_{61}BM$:BL blend films (8.03×10^{-4} for 4% BL, 5.76×10^{-4} for 8% BL, and 3.96×10^{-4} for 16% BL). Although no linear relationship is directly observed between slope and BL content in Figure 5b, the natural logarithm of the slope linearly varies with the natural logarithm of BL content

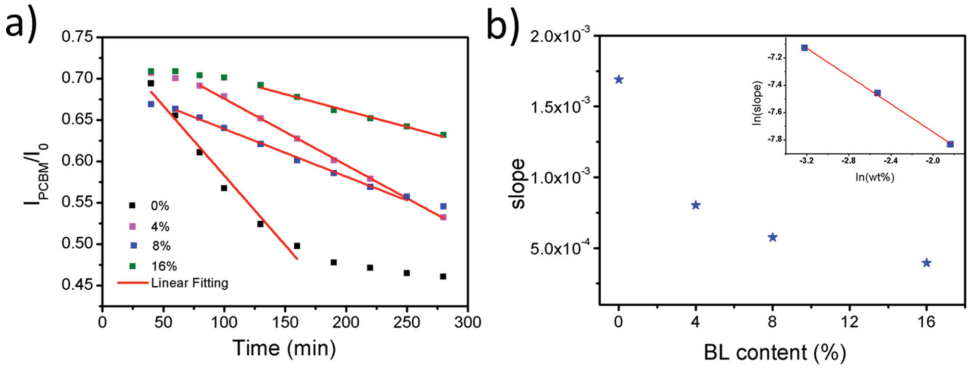

Figure 5. a) Variation in $PC_{61}BM$ absorption ($\lambda = 335$ nm) with annealing time. The slope of linear fitting: 1.69×10^{-3} for P3HT:$PC_{61}BM$, 8.03×10^{-4} for P3HT:$PC_{61}BM$:BL (4%), 5.76×10^{-4} for P3HT:$PC_{61}BM$:BL (8%), and 3.96×10^{-4} for P3HT:$PC_{61}BM$:BL (16%). b) The values of slope as a function of the BL content. Inset is the ln[slope] versus ln[BL content].

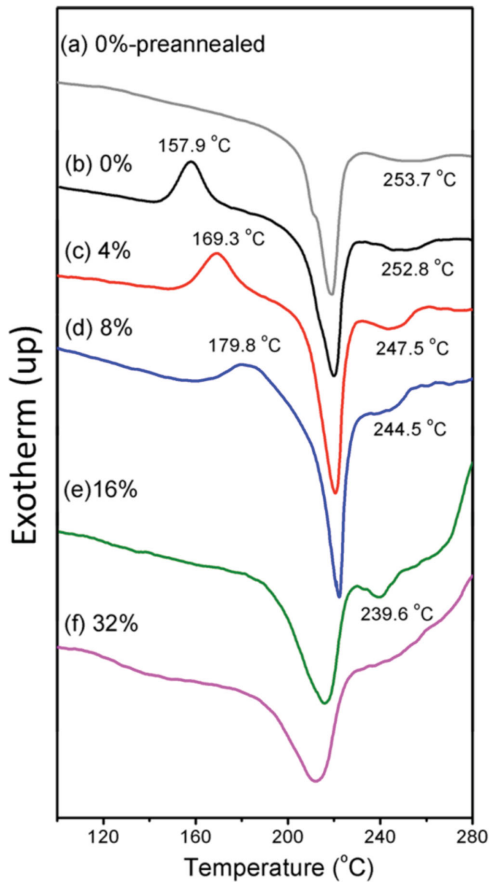

Figure 6. DSC curves of P3HT:$PC_{61}BM$ blend films with different amounts of BL. a) P3HT:$PC_{61}BM$ annealed at 130 °C for 3.5 h, b) P3HT:$PC_{61}BM$, c) P3HT:$PC_{61}BM$:BL (4%), d) P3HT:$PC_{61}BM$:BL (8%), e) P3HT:$PC_{61}BM$:BL (16%), and f) P3HT:$PC_{61}BM$:BL (32%).

$(\ln[\text{slope}] = -8.76 - 0.5\ln[\text{BLcontent}]$, $R = 0.994$, inset in Figure 5b). In other words, in P3HT:$PC_{61}BM$:BL ternary blend system, the growth rate of $PC_{61}BM$ crystals has an inverse relationship with the exponent of BL content.

The effect of BL on $PC_{61}BM$ crystallization behavior in P3HT:$PC_{61}BM$:BL ternary system is further assessed by differential scanning calorimetry (DSC),[26] as shown in **Figure 6**. The sample powders were prepared by drop-casting the solution on glass slide at room temperature, dried in atmosphere for 12 h, and then collected by scratching the sample off the glass slide. For P3HT:$PC_{61}BM$ blend (line b), three peaks are observed: the endothermic one at 220.0 °C is assigned to P3HT melting, the exothermic peak at 157.9 °C, and the endothermic one at 252.7 °C are assigned to the crystallization and melting of $PC_{61}BM$, respectively.[27] This peak assignment can be proved by comparison with the DSC curve of pre-annealed P3HT:$PC_{61}BM$ blend film (130 °C for 3.5 h, line a), in which no $PC_{61}BM$ crystallization peak is observed because the crystallization of $PC_{61}BM$ has already completed during previous annealing. The incorporation of BL obviously changes the positions of crystalline and melting peaks of $PC_{61}BM$. As the BL content increases, the $PC_{61}BM$ crystalline peaks shift to higher temperature: 169.3 °C (4% BL) and 179.8 °C (8% BL), respectively, while such peaks are unobserved for 16% and 32% BL. Correspondingly, the melting peaks shift to lower temperature at 247.5, 244.5, and 239.6 °C for 4%, 8%, and 16% BL, respectively, while no such peak is observed for 32% BL. The changes of the position of $PC_{61}BM$ crystalline and melting peaks are attributed to the supramolecular interaction between $PC_{61}BM$ and BL: more BL in P3HT:$PC_{61}BM$ blend is, more $PC_{61}BM$ molecules interact with BL molecules, resulting in higher thermal energy needed for $PC_{61}BM$ to overcome barrier to crystallize, thus the crystalline peak shifts to higher temperature. In return, the presence of supramolecular interaction leads to the formation of impure $PC_{61}BM$ crystals interspersed with BL, therefore, the melting peak shifts to lower temperature with the increase in BL content. For P3HT:$PC_{61}BM$:BL (16%) blends, the absence of crystalline peak does not imply no $PC_{61}BM$ crystallization during heating because the melting peak of $PC_{61}BM$ is still observed. It is speculated that the crystalline peak perhaps right-shifts to overlap with the P3HT melting peak, leading to the widened P3HT melting region. While for P3HT:$PC_{61}BM$:BL (32%) blend film, both crystalline and melting peaks are unobserved. Two possible reasons are accounted for this: (1) $PC_{61}BM$ does not crystallize during heating; (2) $PC_{61}BM$ crystallizes during heating with its crystalline peak right-shifting and melting peak left-shifting to overlap with the P3HT melting peak. No matter which one is accounted for, it is concluded that $PC_{61}BM$ is more struggling to crystallize with addition of 32% BL.

2.3. Supramolecular Interactions Benefit Stable Percolating Electron Transport Pathways

In photovoltaic devices, the $PC_{61}BM$ component in the active layer carries electron transport.[22] The influence of BL on the electron mobility of P3HT:$PC_{61}BM$ blend film is investigated, and the results are given in **Figure 7** and the processed data are shown in Figure S9, Supporting Information. It can be seen that the electron mobility of the device without thermal annealing monotonically decreases with BL content (from 1.36×10^{-4} cm^2 s^{-1} V^{-1} to 0.46×10^{-4} cm^2 s^{-1} V^{-1}, Figure 7a), which is speculated to be caused by the fact that the $PC_{61}BM$ phase is uniformly dispersed due to the restriction by the BL-C_{60} supramolecular interactions.[24] To investigate the influence of incorporating BL on electron mobility under thermal stress, P3HT:$PC_{61}BM$:BL (8%) devices as well as P3HT:$PC_{61}BM$ devices were thermally annealed at 130 °C for 25 min, 1, and 3 h separately before evaporation of top electrode. It can be seen that the electron mobility for P3HT:$PC_{61}BM$:BL (8%) device increases ceaselessly as thermal annealing time prolonged, reaching 1.91×10^{-4} cm^2 s^{-1} V^{-1} after 3 h heating (Figure 7b). This indicates that a long-time treatment is needed for $PC_{61}BM$ to overcome BL-C_{60} supramolecular attractions and form continuous percolating electron transport pathways. In contrast, the electron mobility for P3HT:$PC_{61}BM$ device increases first to 1.82×10^{-4} cm^2 s^{-1} V^{-1} by short thermal annealing but decreases to 0.36×10^{-4} cm^2 s^{-1} V^{-1} by further heating (Figure 7c). This indicates that good percolating electron transport pathways can be formed by short thermal treatment but deteriorated quickly by a further treatment. It is believed that the different trends of electron mobility as annealing time relates closely to their corresponding morphological stability shown in Figure 3.

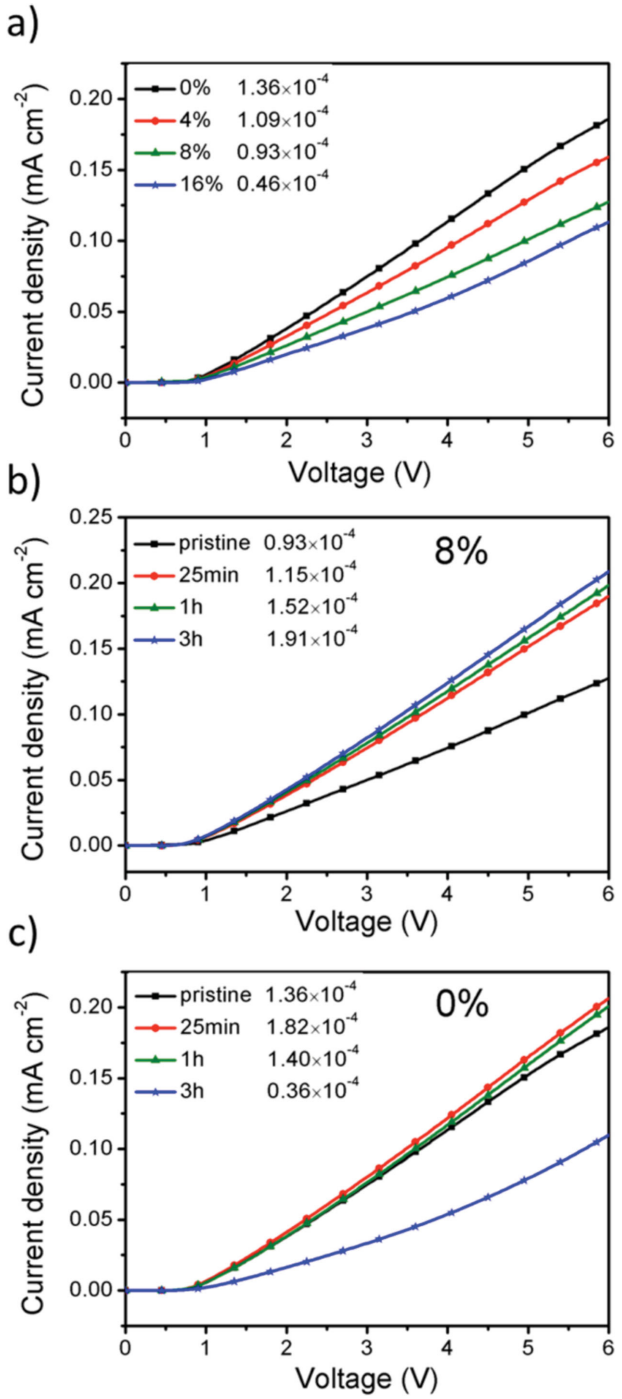

Figure 7. Electron-only devices for: a) P3HT:$PC_{61}BM$ blends with varying BL contents, b) P3HT:$PC_{61}BM$:BL (8%) blends annealed for different times, and c) P3HT:$PC_{61}BM$ blends annealed for different times.

2.4. Supramolecular Interactions Enhance Thermal Stability of PSCs

To investigate the influence of BL incorporation on the thermal stability of photovoltaic devices, a series of devices based on P3HT:$PC_{61}BM$ blend films with different BL content were fabricated. The effect of BL on the stability of PSC devices was investigated by isothermal annealing at 130 °C for different time. Electron buffer layer (LiF) and an aluminum electrode were evaporated onto the active layer after thermal treatment, for eliminating interference of thermal treatment on buffer layer and electrode. The detailed photovoltaic parameters of all the devices are summarized in Tables S1 and S2, Supporting Information. The *J–V* curves (**Figure 8**a) and corresponding photovoltaic parameters in Table S1, Supporting Information, show that the PCE decreases from 3.20% to 2.02% as BL content increases from 0% to 16%. And the decay of PCE values mainly results from the decreased J_{sc} (from 8.83 to 7.72 mA cm^{-2}) and FF (from 67.10% to 51.30%), which can be attributed to the lower electron mobility as discussed above. To exclude the difference in initial efficiency, the relative efficiency η, which is defined as the ratio of PCE_t to PCE_0 (PCE_t and PCE_0 are the efficiencies of the devices with active layers isothermally annealed at 130 °C for t and 25 min, respectively), is used to indicate the maintenance of the device performance instead of absolute efficiency. Figure 8b clearly illustrates that the curve of efficiency decaying as a function of thermal annealing time changes gently for device with higher BL-loading, which indicates that the ability to preserve efficiency becomes stronger. Without addition of BL, the PCE decays rapidly and remains 28.4% (PCE = 0.91%) of the original value after 3 h of heating. In contrast, 12, 24, and more than 48 h of heating are needed for the devices loaded with 2%, 4%, and 8% BL, respectively, to decay to the similar η (Table S2, Supporting Information). A special attention should be paid to device loaded with 8% BL, although the original PCE (2.43%) is lower relative to 3.20% (in case of no BL), it does not decrease after 48 h of heating. Interestingly, its best peak PCE, 2.75%, occurs after 3 h of annealing, which is in good agreement with the fact that the 3 h of heating is needed for the P3HT:$PC_{61}BM$:BL(8%) blend films to form optimized percolating electron transport pathways and achieve a high electron mobility.[28]

The performance data shown in Figure 8b and Table S1, Supporting Information, reveal that the incorporation of BL into P3HT:$PC_{61}BM$ solar cells improves the thermal stability of devices. The performance change is also consistent with the corresponding morphological evolution shown in Figure 3. It is important to note that all the devices were fabricated under the conditions that are optimal for the P3HT:$PC_{61}BM$ blends, which may not be the best for P3HT:$PC_{61}BM$:BL blends. In other words, higher initial efficiencies of the devices incorporated with varied content of BL could be achieved by further optimizing the individual fabrication conditions.

2.5. Mechanism for Enhancement of Thermal Stability

Based on the facts and analysis, a possible mechanism is proposed for the morphological evolution of P3HT:$PC_{61}BM$ and P3HT:$PC_{61}BM$:BL blend films,[29] as given in **Figure 9**. Upon thermal annealing of the as-cast P3HT:$PC_{61}BM$ thin film at 130 °C for 25 min, the $PC_{61}BM$ molecules, originally dispersed and intercalated in the P3HT domains (Figure 9a_0), can freely diffuse out of these mixed regions to aggregate into pure $PC_{61}BM$ clusters. The $PC_{61}BM$ diffusion induces simultaneously more ordered packing of P3HT, leading to an optimized

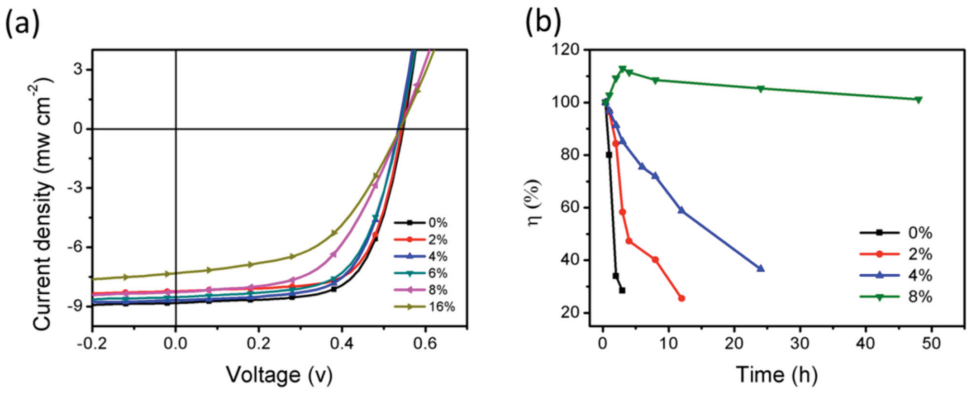

Figure 8. a) *J–V* characteristics of PSCs based on P3HT:$PC_{61}BM$ loading different contents of BL after isothermal annealing at 130 °C for 25 min. b) Relative efficiency of P3HT:$PC_{61}BM$ devices loading different contents of BL as a function of annealing time.

morphology for efficient exciton dissociation and charge transport (Figure 9b_0). However, over-long thermal annealing causes the formation of large size $PC_{61}BM$ aggregates, which reduces the percolating electron transport pathways within the mixed regions and thus increases the charge recombination losses (Figure 9c_0). Therefore, although the P3HT:$PC_{61}BM$ device delivers the highest PCE value of 3.2% at the beginning, its morphological stability, electron mobility, and device performance against heating turns out to be the worst.

For the as-cast P3HT:$PC_{61}BM$:BL (8%) blend films, the $PC_{61}BM$ molecules are hard to move and aggregate due to BL-C_{60} supramolecular interactions (Figure 9a_2), thus the pre-annealing for 25 min at 130 °C is not enough to reach the optimal morphology (Figure 9b_2). By further heating for 3 h, the $PC_{61}BM$ molecules gradually aggregate into $PC_{60}BM$ clusters with concomitant enhancement of P3HT crystallinity (Figure 9c_2), reaching its best morphological state and gaining its highest efficiency. This also improves the percolating electron transport pathways within the mixed regions. Although the device P3HT:$PC_{61}BM$:BL (8%) delivers an unsatisfactory PCE value at the beginning due to the unoptimized morphology, its morphological stability against heating turns out to be the best.

For the as-cast P3HT:$PC_{61}BM$:BL (4%) blend film (Figure 9a_1), on one hand, the pre-annealing at 130 °C for 25 min is not enough for reaching the optimal morphology referred to P3HT:$PC_{61}BM$ blend film due to the BL-$PC_{61}BM$ interactions

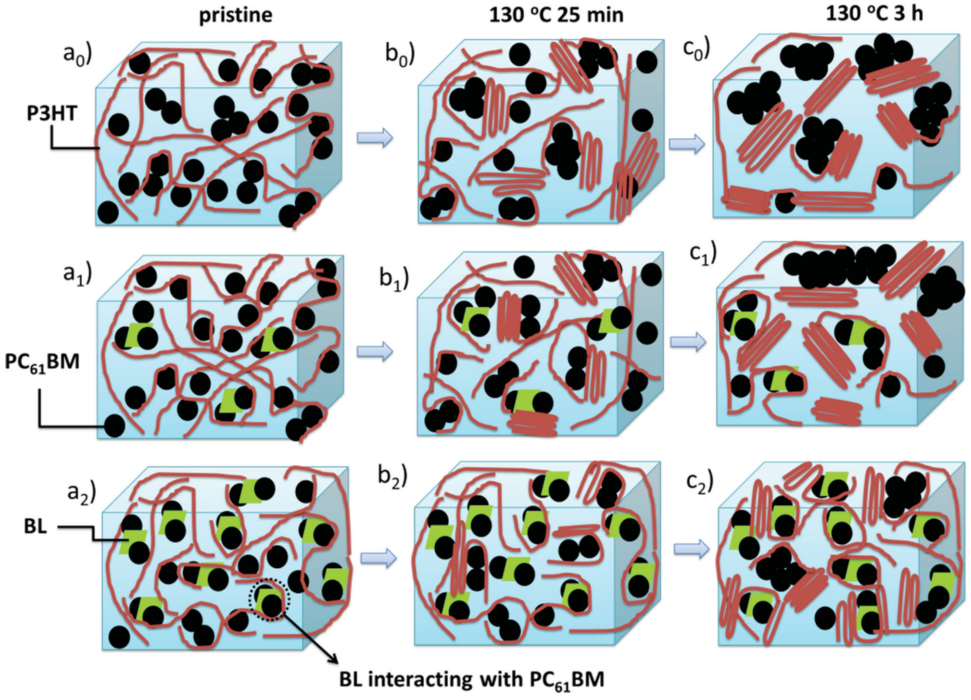

Figure 9. Morphological evolutions of P3HT:$PC_{61}BM$ blend with different content of BL. a_0–c_0) unstable morphology of a P3HT:$PC_{61}BM$ binary blend against thermal annealing, a_1–c_1) less stable morphology of a P3HT:$PC_{61}BM$:BL (4%) ternary blend against thermal annealing, a_2–c_2) stable morphology of a P3HT:$PC_{61}BM$:BL (8%) ternary blend against thermal annealing.

(Figure 9b$_1$). On the other hand, the annealing of 3 h, which is best for P3HT:PC$_{61}$BM:BL (8%), is too long because no so much BL-PC$_{61}$BM interactions exist. In other words, their optimal thermal annealing time should be between 25 min and 3 h.

2.6. Applicability of Porphyrin

From above we can see that the porphyrin with the given structure significantly increases the thermal stability of P3HT:PC$_{61}$BM based PSC device. In fact, this method could also be applied to other porphyrins. For example, our preliminary data show that the porphyrins with different core metal ions (Mn, Zn, Cu) and substituted groups (nitro, 4-chloro-octafluorobutyl) have different effects on the performance of P3HT:PC$_{61}$BM devices: some of them with specific structure not only maintain the original PCE (3.14%–3.34%), but also keep the values unchanged up to 3 h at 130 °C. Furthermore, encouraging results also emerge for low band gap based devices (all these data will be reported later). Therefore, this strategy of incorporating porphyrin into active layer to increase the PSC thermal stability is universal and would show great potentials in scientific research and real application of polymer solar cells.

3. Conclusion

In this paper, the porphyrin compound is smartly utilized as a new kind of additive materials to control BHJ morphology and enhance the thermal stability of PSCs. It is found that the BL could effectively suppress the n-type PC$_{61}$BM materials from extensive thermal-driven aggregation to overcome the morphological instability through supramolecular BL-PC$_{61}$BM interactions. The extent of the physical interaction can be adjusted by simply varying the content of porphyrin. In PC$_{61}$BM: BL binary system, PC$_{61}$BM could not crystallize by addition of 0.5 equivalent amount of BL even after 36 h of heating at 150 °C. In P3HT:PC$_{61}$BM:BL ternary system, the effect of BL on the morphological stability is reflected from the mitigated morphological evolution, reduced rate of PC$_{61}$BM crystallization, and increased crystallization and decreased melting temperature of PC$_{61}$BM, respectively, which heavily depends on BL content. This stabilized morphology is of beneficial for devices maintaining high electron mobility and favorable performance even after a long-time heating. For example, doping 8% porphyrin BL (relative to the weight of PC$_{61}$BM) makes the device only decaying 10.5% of its original PCE after 48 h of annealing at 130 °C, while no BL addition results in 71.5% decaying after only 3 h of annealing. Our preliminary data show that this strategy could also be applied to other porphyrins. Given the nature of supramolecular interaction (π-system of porphyrin interacting with π-system of C$_{60}$ cage), it is reasonable that this strategy will promote the extensive application of other macrocyclic compounds to achieve stabilization of PSCs.

4. Experimental Section

Materials: Poly(3-hexylthiophene) (P3HT) used in this study was successfully synthesized via Grim polymerization, and the number-average molecular weight (M_n) was estimated by gel permeation chromatography (GPC) to be around 55000 g mol^{-1} with a polydispersity index (PDI) value of 1.43, a regioregularity value of 98.2%. All the porphyrins were kindly supported by Guoyong's group, Shanghai Institute of Organic Chemistry, CAS. [6, 6]-phenyl-C61-butyric acid methyl ester (PC$_{61}$BM) (99.5%) and *o*-dichlorobenzene (ODCB, anhydrous, 99%) were acquired from Sigma-Aldrich Co.

Film Preparation and Characterization: Neat PC$_{61}$BM film, neat BL film, and PC$_{61}$BM:BL blend films were spun-cast onto clean and dried glass slides at 450 rpm for 5 min from PC$_{61}$BM/ODCB (20 mg mL^{-1}), BL/ODCB (10 mg mL^{-1}) and PC$_{61}$BM:BL (1:*x*, in weight, total concentration of 20 mg mL^{-1})/ODCB solutions separately. P3HT:PC$_{61}$BM:BL (1:1:*x*, in weight) films were spun-cast onto clean and dried glass slides at 700 rpm for 5min from corresponding solutions (all P3HT concentration was fixed at 20 mg mL^{-1}). Thermal treatments were applied under nitrogen atmosphere. Absorption spectra were collected on a Lambda 750 spectrometer (Perkin-Elmer, Wellesley, MA). Optical microscopy investigations were carried out by a Carl Zeiss A1m microscope equipped with infinity 4–11 digital camera from Lumenera Corporation, Canada. Fluorescence emission spectra were obtained with an Edinburgh FLS 920. X-ray diffraction (XRD) profiles were obtained using a Bruker D8 Discover Reflector with X-ray generation power of 40 kV tube voltage and 40 mA tube current. The samples were scanned in detector scan mode across a range of $2\theta = 2°–30°$ with a step size of 0.05° and a counting period of 5 step s^{-1}. Surface morphology of the film was characterized on an Agilent 5500 AFM by tapping mode in ambient atmosphere. Differential scanning calorimetry (DSC) was measured on TA Q100 instrument under atmosphere at a heating rate of 5 °C min^{-1}.

Device Fabrication and Characterization: The glass-indium tin oxide (ITO) substrates (obtained from Lumtec, 7 Ω sq^{-1}) were first cut into 3.0 × 3.0 cm and patterned by lithograph, then were ultrasonically washed by detergent, de-ionic water, acetone, and isopropanol sequentially for 25 min/each and subsequently exposed to UV–ozone for 25 min. Poly(3,4-ethylenedioxy-thiophene):poly (styrene-sulfonate) (PEDOT:PSS, Baytron PVPAI 4083) was passed through a 0.45 μm filter before deposition on ITO with a thickness around 30 nm by spin coating at 3000 rpm and dried at 150 °C for 20 min in the air. Active-layer solutions of P3HT:PC$_{61}$BM blends with various amounts of BL in ODCB were prepared. The weight ratio of P3HT to PC$_{61}$BM was fixed at 1:1 and the concentration of P3HT was kept at 20 mg mL^{-1}. The solutions were stirred at 60 °C for 12 h in air, and then spin-coated at a speed rate of 700 rpm for 2.5 min on the top of PEDOT:PSS layer under nitrogen atmosphere (the film thickness was about 170 nm). After that, the film was baked at 130 °C for different periods of time to give a series of active layers with different degree of thermal annealing. Subsequently the device was completed by thermal evaporation of LiF (0.8 nm) and Al (100 nm) under <1 × 10^{-5} Torr pressure. All the active area of the device is 9 mm^2. The current–voltage (*J*–*V*) measurement of the polymer photovoltaic cells was conducted immediately in glovebox by a computer-controlled Keithley 2400 Source Measurement Unit (SMU) with a Peccell solar simulator under the illumination of AM1.5G, 100 mW cm^{-2}. The electron mobilities were measured by the space charge limited current (SCLC) method on an electron-only device with a structure of ITO/TIPD (titanium (diisopropoxide) bis(2,4-pentanedionate), its chemical structure illustrated in Scheme S1, Supporting Information)/active layer/Ca/Al. SCLC device fabrication was almost the same as device fabrication, except the bottom electrode was changed from PEDOT:PSS to TIPD and the film thickness was about 100 nm. The measurement of electron mobilities was conducted in the dark on a computer-controlled Keithley 2400 SMU. The SCLC mobility was estimated following the Mott-Gurney square law $J = 9(\varepsilon_0\varepsilon_r\mu)/8\times(V^2/d^3)$, where J is current density, ε_0 is the permittivity of vacuum, ε_r is dielectric constant of the fullerene derivatives, μ is hole mobility, and d is film thickness.

Supporting Information

Supporting Information is available from the Wiley Online Library or from the author.

Acknowledgements

This work was supported by the National Natural Science Foundation of China (Grant No. 20990233), Hi-Tech Research and Development Program (863) of China (Grant No. 2011AA050524), Solar Energy Initiative (KGCX2-YW- 399 + 9) of the Chinese Academy of Sciences. X.Y. would also like to thank the Fund for Distinguished Young Scholars (20925415) of NSFC. The author also thanks Dr. Shuai Zhao for material supply.

Received: September 1, 2014
Revised: October 23, 2014
Published online: December 16, 2014

[1] a) T. Earmme, Y.-J. Hwang, N. M. Murari, S. Subramaniyan, S. A. Jenekhe, *J. Am. Chem. Soc.* **2013**, *135*, 14960; b) Y. Liang, Z. Xu, J. Xia, S.-T. Tsai, Y. Wu, G. Li, C. Ray, L. Yu, *Adv. Mater.* **2010**, *22*, E135; c) J. H. Seo, A. Gutacker, Y. Sun, H. Wu, F. Huang, Y. Cao, U. Scherf, A. J. Heeger, G. C. Bazan, *J. Am. Chem. Soc.* **2011**, *133*, 8416; d) G. Dennler, M. C. Scharber, C. J. Brabec, *Adv. Mater.* **2009**, *21*, 1323.

[2] Z. He, C. Zhong, S. Su, M. Xu, H. Wu, Y. Cao, *Nat. Photonics* **2012**, *6*, 591.

[3] J. You, L. Dou, K. Yoshimura, T. Kato, K. Ohya, T. Moriarty, K. Emery, C.-C. Chen, J. Gao, G. Li, Y. Yang, *Nat. Commun.* **2013**, *4*, 1446.

[4] M. T. Dang, L. Hirsch, G. Wantz, *Adv. Mater.* **2011**, *23*, 3597.

[5] a) N. Espinosa, M. Hosel, M. Jorgensen, F. C. Krebs, *Energy Environ. Sci.* **2014**, *7*, 855; b) R. Gupta, S. Walia, M. Hosel, J. Jensen, D. Angmo, F. C. Krebs, G. U. Kulkarni, *J. Mater. Chem. A* **2014**, *2*, 10930.

[6] M. Jørgensen, K. Norrman, S. A. Gevorgyan, T. Tromholt, B. Andreasen, F. C. Krebs, *Adv. Mater.* **2012**, *24*, 580.

[7] a) J. Y. Kim, S. H. Kim, H. H. Lee, K. Lee, W. Ma, X. Gong, A. J. Heeger, *Adv. Mater.* **2006**, *18*, 572; b) D. Angmo, P. M. Sommeling, R. Gupta, M. Hösel, S. A. Gevorgyan, J. M. Kroon, G. U. Kulkarni, F. C. Krebs, *Adv. Eng. Mater.* **2014**, *16*, 976.

[8] J. M. Y. Carrillo, R. Kumar, M. Goswami, B. G. Sumpter, W. M. Brown, *Phys. Chem. Chem. Phys.* **2013**, *15*, 17873.

[9] S. Khelifi, E. Voroshazi, D. Spoltore, F. Piersimoni, S. Bertho, T. Aernouts, J. Manca, J. Lauwaert, H. Vrielinck, M. Burgelman, *Sol. Energy Mater. Sol. Cells* **2014**, *120*, 244.

[10] C. J. Schaffer, C. M. Palumbiny, M. A. Niedermeier, C. Jendrzejewski, G. Santoro, S. V. Roth, P. Müller-Buschbaum, *Adv. Mater.* **2013**, *25*, 6760.

[11] a) K. Sivula, C. K. Luscombe, B. C. Thompson, J. M. J. Fréchet, *J. Am. Chem. Soc.* **2006**, *128*, 13988; b) C. H. Woo, B. C. Thompson, B. J. Kim, M. F. Toney, J. M. J. Fréchet, *J. Am. Chem. Soc.* **2008**, *130*, 16324.

[12] a) J. Y. Oh, M. Shin, T. I. Lee, W. S. Jang, Y.-J. Lee, C. S. Kim, J.-W. Kang, J.-M. Myoung, H. K. Baik, U. Jeong, *Macromolecules* **2013**, *46*, 3534; b) L. Li, D. L. Jacobs, Y. Che, H. Huang, B. R. Bunes, X. Yang, L. Zang, *Org. Electron.* **2013**, *14*, 1383.

[13] a) X. Meng, W. Zhang, Z. A. Tan, Y. Li, Y. Ma, T. Wang, L. Jiang, C. Shu, C. Wang, *Adv. Funct. Mater.* **2012**, *22*, 2187; b) H.-W. Liu, D.-Y. Chang, W.-Y. Chiu, S.-P. Rwei, L. Wang, *J. Mater. Chem.* **2012**, *22*, 15586.

[14] a) K. Sivula, Z. T. Ball, N. Watanabe, J. M. J. Fréchet, *Adv. Mater.* **2006**, *18*, 206; b) J.-H. Tsai, Y.-C. Lai, T. Higashihara, C.-J. Lin, M. Ueda, W.-C. Chen, *Macromolecules* **2010**, *43*, 6085; c) Y.-C. Lai, T. Higashihara, J.-C. Hsu, M. Ueda, W.-C. Chen, *Sol. Energy Mater. Sol. Cells* **2012**, *97*, 164.

[15] a) C.-Y. Chang, C.-E. Wu, S.-Y. Chen, C. Cui, Y.-J. Cheng, C.-S. Hsu, Y.-L. Wang, Y. Li, *Angew. Chem. Int. Ed.* **2011**, *50*, 9386; b) S. Miyanishi, K. Tajima, K. Hashimoto, *Macromolecules* **2009**, *42*, 1610; c) F. Ouhib, M. Tomassetti, J. Manca, F. Piersimoni, D. Spoltore, S. Bertho, H. Moons, R. Lazzaroni, S. Desbief, C. Jerome, C. Detrembleur, *Macromolecules* **2013**, *46*, 785; d) L. Derue, O. Dautel, A. Tournebize, M. Drees, H. Pan, S. Berthumeyrie, B. Pavageau, E. Cloutet, S. Chambon, L. Hirsch, A. Rivaton, P. Hudhomme, A. Facchetti, G. Wantz, *Adv. Mater.* **2014**, *26*, 5831.

[16] a) A. Moujoud, S. H. Oh, J. J. Hye, H. J. Kim, *Sol. Energy Mater. Sol. Cells* **2011**, *95*, 1037; b) Y.-J. Cheng, C.-H. Hsieh, P.-J. Li, C.-S. Hsu, *Adv. Funct. Mater.* **2011**, *21*, 1723; c) Y.-H. Chen, P.-T. Huang, K.-C. Lin, Y.-J. Huang, C.-T. Chen, *Org. Electron.* **2012**, *13*, 283.

[17] a) U. Jimenez Castillo, P. Guadarrama, S. Fomine, *Org. Electron.* **2013**, *14*, 2617; b) E. Dietel, A. Hirsch, E. Eichhorn, A. Rieker, S. Hackbarth, B. Roder, *Chem. Commun.* **1998**, *18*, 1981.

[18] a) D. M. Lyons, J. Kesters, W. Maes, C. W. Bielawski, J. L. Sessler, *Synth. Met.* **2013**, *178*, 56; b) A. Ltaief, R. Ben Chaâbane, A. Bouazizi, J. Davenas, *Mater. Sci. Eng., C* **2006**, *26*, 344.

[19] T. Hasobe, P. V. Kamat, V. Troiani, N. Solladié, T. K. Ahn, S. K. Kim, D. Kim, A. Kongkanand, S. Kuwabata, S. Fukuzumi, *J. Phys. Chem. B* **2004**, *109*, 19.

[20] a) U. J. Castillo, P. Guadarrama, S. Fomine, *Org. Electron.* **2013**, *14*, 2617; b) T. Ishi-i, R. Iguchi, E. Snip, M. Ikeda, S. Shinkai, *Langmuir* **2001**, *17*, 5825.

[21] a) M. Vizuete, M. J. Gómez-Escalonilla, J. L. G. Fierro, P. Atienzar, H. García, F. Langa, *ChemPhysChem* **2014**, *15*, 100; b) D. Gust, T. A. Moore, A. L. Moore, D. Kuciauskas, P. A. Liddell, B. D. Halbert, *J. Photochem. Photobiol. B: Biol.* **1998**, *43*, 209; c) A. Mondal, K. Santhosh, A. Bauri, S. Bhattacharya, *Spectrochim. Acta Part A* **2014**, *121*, 559.

[22] W.-R. Wu, U. S. Jeng, C.-J. Su, K.-H. Wei, M.-S. Su, M.-Y. Chiu, C.-Y. Chen, W.-B. Su, C.-H. Su, A.-C. Su, *ACS Nano* **2011**, *5*, 6233.

[23] K. T. Nielsen, H. Spanggaard, F. C. Krebs, *Macromolecules* **2005**, *38*, 1180.

[24] a) J. E. Carle, B. Andreasen, T. Tromholt, M. V. Madsen, K. Norrman, M. Jorgensen, F. C. Krebs, *J. Mater. Chem.* **2012**, *22*, 24417; b) M. Helgesen, J. E. Carlé, J. Helt-Hansen, A. Miller, F. C. Krebs, *J. Appl. Polym. Sci.* **2014**, *131*, 40795.

[25] J. J. Richards, A. H. Rice, R. D. Nelson, F. S. Kim, S. A. Jenekhe, C. K. Luscombe, D. C. Pozzo, *Adv. Funct. Mater.* **2013**, *23*, 514.

[26] F. Machui, S. Rathgeber, N. Li, T. Ameri, C. J. Brabec, *J. Mater. Chem.* **2012**, *22*, 15570.

[27] J. Zhao, A. Swinnen, G. Van Assche, J. Manca, D. Vanderzande, B. V. Mele, *J. Phys. Chem. B* **2009**, *113*, 1587.

[28] D. Chirvase, J. Parisi, J. C. Hummelen, V. Dyakonov, *Nanotechnology* **2004**, *15*, 1317.

[29] M.-H. Liao, C.-E. Tsai, Y.-Y. Lai, F.-Y. Cao, J.-S. Wu, C.-L. Wang, C.-S. Hsu, I. Liau, Y.-J. Cheng, *Adv. Funct. Mater.* **2014**, *24*, 1418.